Unconditional Quantum Teleportation

A. Furusawa, J. L. Sørensen, S. L. Braunstein, C. A. Fuchs, H. J. Kimble,* E. S. Polzik

Quantum teleportation of optical coherent states was demonstrated experimentally using squeezed-state entanglement. The quantum nature of the achieved teleportation was verified by the experimentally determined fidelity $F^{exp} = 0.58 \pm 0.02$, which describes the match between input and output states. A fidelity greater than 0.5 is not possible for coherent states without the use of entanglement. This is the first realization of unconditional quantum teleportation where every state entering the device is actually teleported.

Quantum teleportation is the disembodied transport of an unknown quantum state from one place to another (*1*). All protocols for accomplishing such transport require nonlocal correlations, or entanglement, between systems shared by the sender and receiver. John Bell's famous theorem on the incompatibility of quantum mechanics with local hidden variable theories establishes that entanglement represents the quintessential distinction between classical and quantum physics (*2*). Recent advances in the burgeoning field of quantum information have shown that entanglement is also a valuable resource that can be exploited to perform otherwise impossible tasks, of which quantum teleportation is the prime example.

Teleportation of continuous quantum variables. To date, most attention has focused on teleporting the states of finite-dimensional systems, such as the two polarizations of a photon or the discrete level structure of an atom (*1, 3–8*). However, quantum teleportation is also possible for continuous variables corresponding to states of infinite-dimensional systems (*9, 10*), such as optical fields or the motion of massive particles (*11*). The particular implementation of teleported optical fields is noteworthy in four ways. First, the relevant optical tools are powerful and well suited for integration into an evolving communication technology. Second, these methods apply to other quantum computational protocols, such as quantum error correction for continuous variables using linear optics (*12*) and superdense coding of optical information (*13*). Third, finite-dimensional systems can always be considered as subsystems of infinite-dimensional systems where the above advantages can be put to use. Finally, a relatively simple design is implemented that eliminates the need for some nonlinear operations (*10*); these nonlinear operations constitute the main bottleneck to the efficacy of other teleportation schemes.

This teleportation scheme uses the protocol described in (*10*). The experimental setup (Fig. 1) consists of a sending station operated by Alice, a receiving station operated by Bob, and a station for producing beams of entangled photons [labeled EPR (Einstein-Podolsky-Rosen) beams (1, 2)]. Alice and Bob each receive half of the EPR photons. Alice's station consists of two homodyne detectors $D_{x,p}$ (including two local oscillators $LO_{x,p}$), where x and p denote the real and imaginary components of the (complex) electric field. These detectors measure an entangled combination of the input state $|v_{in}\rangle$ and Alice's half of the EPR beam. Classical lines of communication are used to transmit Alice's measurement results to Bob, who then uses that information to transform the second half of the EPR beam (at the mirror m_{Bob}) into an output $\hat{\rho}_{out}$ that closely mimics the original unknown input.

In our scheme, a third party, Victor (the verifier), prepares an initial input in the form of a coherent state of the electromagnetic field $|v_{in}\rangle$, which he then passes to Alice for teleportation. Likewise, the teleported field that emerges from Bob's sending station is interrogated by Victor to verify that teleportation has actually taken place: At this stage, Victor records the amplitude and variance of the field generated by Bob, and is thereby able to assess the "quality" of the teleportation protocol. This is done by determining the overlap between input and output as given by the fidelity $F \equiv \langle v_{in}|\hat{\rho}_{out}|v_{in}\rangle$. As discussed below, for the teleportation of coherent states, $F_c = 0.5$ sets a boundary for entrance into the quantum domain in the sense that Alice and Bob can exceed this value only by making use of entanglement (*14*). From Victor's measurements of orthogonal quadratures (see below), our experiment achieves $F^{exp} = 0.58 \pm 0.02$ for the field emerging from Bob's station, thus demonstrating the nonclassical character of this experimental implementation.

To describe the infinite-dimensional states of optical fields, it is convenient to introduce a pair (x, p) of continuous variables of the electric field, called the quadrature-phase amplitudes (QAs), that are analogous to the canonically conjugate variables of position and momentum of a massive particle (*15*). In terms of this analogy, the entangled beams shared by Alice and Bob have nonlocal correlations similar to those first described by Einstein *et al*. (*16*). The requisite EPR state is efficiently generated via the nonlinear optical process of parametric down-conversion previously demonstrated in (*17*). The resulting state corresponds to a squeezed two-mode optical field. In the ideal case, namely perfect EPR correlations and lossless propagation and detection, the teleported state emerges from Bob's station with perfect fidelity $F = 1$ (*10*).

Apart from the advantages of continuous quantum variables, our experiment is significant in that it attains full teleportation as originally envisioned in (*1*). This is in contrast to previous teleportation experiments where no physical state enters the device from the outside (*7*) or where the teleported state is destroyed at Bob's station (*8*), never emerging for subsequent exploitation (*18*). Furthermore, in both these previous experiments, there never exists an actual physical field with high (nonclassical) teleportation fidelity at the output.

Apparatus and protocol. As illustrated in Fig. 1, entangled EPR beams are generated along paths {1, 2} by combining two independent squeezed beams at a 50/50 beam splitter (*19*), with the relative phase between the squeezed fields actively servo-controlled. The squeezed fields are themselves produced by parametric down-conversion in a subthreshold optical parametric oscillator (OPO) (*20*). The particular setup is as described in (*21*), save one important exception. Because the cavity for the OPO is a traveling-wave resonator (that is, a folded-ring geometry), it is possible to drive the intracavity nonlinear crystal with two counterpropagating pump beams to generate two (nominally) independent squeezed fields countercirculating within the cavity and emerging along the separate paths {*i*, *ii*} (see Fig. 1). Note that the light from a single-frequency titanium sapphire ($TiAl_2O_3$) laser at 860 nm serves as the primary source for all fields in our experiment. Ninety percent of the laser output at frequency ω_L is directed to a frequency-doubling cavity to generate roughly 300 mW of blue light at $2\omega_L$ (*22*), with this output then split into two beams that serve as harmonic pumps for (degenerate) parametric down-conversion, $2\omega_L \rightarrow \omega_L \pm \Omega$, within the OPO. Both

A. Furusawa, C. A. Fuchs, H. J. Kimble are in the Norman Bridge Laboratory of Physics, California Institute of Technology, Pasadena, CA 91125, USA. J. L. Sørensen and E. S. Polzik are at the Institute of Physics and Astronomy, Aarhus University, Aarhus 8000, Denmark. S. L. Braunstein is at the School of Electrical Engineering and Computer Systems, University of Wales, Bangor LL57 1UT, UK.

*To whom correspondence should be addressed. E-mail: hjkimble@cco.caltech.edu

the doubling cavity and the cavity of the OPO contain an *a*-cut potassium niobate ($KNbO_3$) crystal for temperature-tuned, noncritical phase matching, with the lengths of both cavities under servo-control to maintain resonance for a TEM_{00} longitudinal mode.

Our protocol is as follows: EPR beam 1 (Fig. 1) propagates to Alice's sending station, where it is combined at a 50/50 beam splitter with the unknown input state $|v_{in}\rangle$, which is a coherent state of complex amplitude $v_{in} \equiv x_{in} + ip_{in}$. Alice uses two sets of balanced homodyne detectors (D_x, D_p) to make a "Bell-state" measurement of the amplitudes $x = (x_{in} - x_1)/\sqrt{2}$ and $p = (p_{in} + p_1)/\sqrt{2}$ for the input state and the EPR field 1 of amplitude $\alpha_1 \equiv x_1 + ip_1$. The classical (photocurrent) outcomes are denoted by (i_x, i_p) respectively, and are scaled to (x, p). At unit efficiency, such detectors provide "optimal" information about (x, p) via (i_x, i_p) (*23–25*), with the knowledge gained about the unknown input state $|v_{in}\rangle$ going to zero as $\sigma^{-}_{i,ii} \rightarrow 0$, where $\sigma^{-}_{i,ii}$ denotes the variances of squeezed QAs of the fields along paths {i, ii}.

Because of the entanglement between the EPR beams {1, 2}, Alice's Bell-state detection collapses Bob's field 2 into a state conditioned on the measurement outcome (i_x, i_p). Hence, after receiving this classical information from Alice, Bob is able to construct the teleported state $\hat{\rho}_{out}$ via a simple phase-space displacement of the EPR field 2 (*26*). In our experiment, the amplitude and phase modulators (M_x, M_p) shown in Fig. 1 transform the (amplified) photocurrents (i_x, i_p) into a complex field amplitude, which is then combined with the EPR beam 2 at the mirror m_{Bob} of reflectivity 0.99. In this manner, we affect the displacement $\alpha_2 \rightarrow v_{out} = \alpha_2 + g\sqrt{2}(i_x + ii_p) = gv_{in} + [(x_2 - gx_1) + i(p_2 + gp_1)]$, where g describes Bob's (suitably normalized) gain for the transformation from photocurrent to output field. In the limit $\sigma^{-}_{i,ii} \rightarrow 0$, $(x_1 - x_2, p_1 + p_2) \rightarrow 0$ [that is, the EPR beams become "quantum copies" of each other with respect to their QAs (*19*)], so that for $g = 1$, $\hat{\rho}_{out} \rightarrow |v_{in}\rangle\langle v_{in}|$, resulting in perfect teleportation with fidelity $F \rightarrow 1$.

Quantum versus classical teleportation. Of course, the limit $F = 1$ is reached only for ideal (singular) EPR correlations and for lossless propagation and detection. To aid in quantifying the "quality" of teleportation in our actual experiment, we calculate F for the case of a finite degree of EPR correlation and in the presence of non-unit efficiencies, which for a coherent-state input $|v_{in}\rangle$ becomes

$$F = 2/\sigma_Q \exp[-2|v_{in}|^2(1-g)^2/\sigma_Q] \quad (2)$$

(*14*), where σ_Q is the variance of the Q function of the teleported field, given by

$$\sigma_Q = 1 + g^2 + (\sigma^{-}/2)(g\xi_1 + \xi_2)^2 + (\sigma^{+}/2)(g\xi_1 - \xi_2)^2 + (1 - \xi_1^2)g^2 + (1 - \xi_2^2) + 2g^2(1/\eta^2) - 1) \quad (2)$$

Here, $\sigma^{\pm}$ are the variances of the amplified/squeezed QAs that are summed to form the EPR beams (assuming $\sigma^{\pm}_i = \sigma^{\pm}_{ii}$), $\xi_{1,2}$ characterize the (amplitude) efficiency with which the EPR beams are propagated and detected along paths {1, 2}, and η gives the (amplitude) efficiency for detection of the unknown input state by Alice (*10*).

Classical teleportation replaces the EPR beams by (uncorrelated) vacuum inputs ($\sigma^{\pm} \rightarrow 1$), thus eliminating the shared entanglement between Alice and Bob. For coherent states distributed across the complex plane, optimum fidelity is achieved for $g \approx 1$, in which case $(\sigma_Q - 1) = \sigma_W \geq 3$ and $F \leq 0.5$, and equality is obtained only for $\eta = 1$. In this case, one unit of vacuum noise in the variance σ_W of the Wigner distribution arises from the original coherent-state input ($\sigma_{in} = 1$), whereas the other two units are the so-called quantum duties (or quduties) that must be paid at each crossing of the border between quantum and classical domains (*10*). One quduty arises from Alice's attempt to infer both QAs of the field (*23*); the other quduty results from Bob's displacement.

However, quantum teleportation should necessarily require Alice and Bob to share a nonlocal quantum resource, such as the EPR beams in our experiment. The question of the operational verification of this shared entanglement is relevant not only to our teleportation protocol, but also to eavesdropping in quantum cryptography (*27*). So long as Alice and Bob can communicate only over a classical channel, we have shown that for $g = 1$, $\sigma_W > \sigma_{in} + 2$, so that $\sigma^{c}_W = 3$ heralds the boundary between quantum and classical teleportation for coherent-state inputs. More generally, even in the absence of loss, Alice and Bob can achieve $F > 1/2$ for an unknown coherent state only by way of shared quantum entanglement, as can be operationally (and independently) verified by Victor (*14*). Note that for experiments involving photon polarization as in (*7, 8*), the corresponding fidelity threshold for a completely unknown quantum state is $F > 2/3$ (*28*), which could not be approached because of the low detection efficiencies. Moreover, in contrast to the work in (*7, 8*), Victor need not to make any arrangement with Alice and Bob in order to make an objective assessment of the quantum nature of the teleportation process.

Experimental results. We concentrate first on Alice's measurement of the unknown input state (Fig. 2). The spectral density of photocurrent fluctuations $\Psi_x^{Alice}(\Omega)$, recorded by Alice's balanced homodyne detector D_x as the phase ϕ_{in} of the coherent-state input [$v_{in} = |v_{in}|\exp(i\phi_{in})$] is swept linearly by Victor, is shown in Fig. 2A. For $\phi_{in} - \theta_{A,x} = p\pi$ (with integral p and $\theta_{A,x}$ as the phase of local oscillator at D_x), $\Psi_x^{Alice}(\Omega)$ rises to a maximum, while for half-integral p it falls to a minimum that is set by the variance of EPR beam 1. A completely analogous set of traces is obtained for the output from Alice's detector D_p, except now shifted in phase by $\pi/2$ in correspondence to the fact that phases of the local oscillator beams at (D_x, D_p) are fixed to be in quadrature by active servo-control. For $v_{in} = 0$, the phase-insensitive noise levels shown in Fig. 2A correspond to the case of no EPR beams present [that is, $\sigma^{\pm}_{i,ii} \rightarrow 1$, giving the vacuum-state level $\Phi_{0,x}^{Alice}(\Omega)$] and to that with the EPR beam 1 distributed to Alice [excess noise at the level $\Lambda_x^{Alice}(\Omega)$]. A more detailed view of these noise levels is provided in Fig. 2B. The observed increases in photocurrent fluctuations from $\Phi_{0,(x,p)}^{Alice} \rightarrow \Lambda_{(x,p)}^{Alice}$ represent the necessary degradation in signal-to-noise ratio for Alice that accompanies quantum teleportation, with $\Lambda_{(x,p)}^{Alice} \rightarrow \infty$ in the

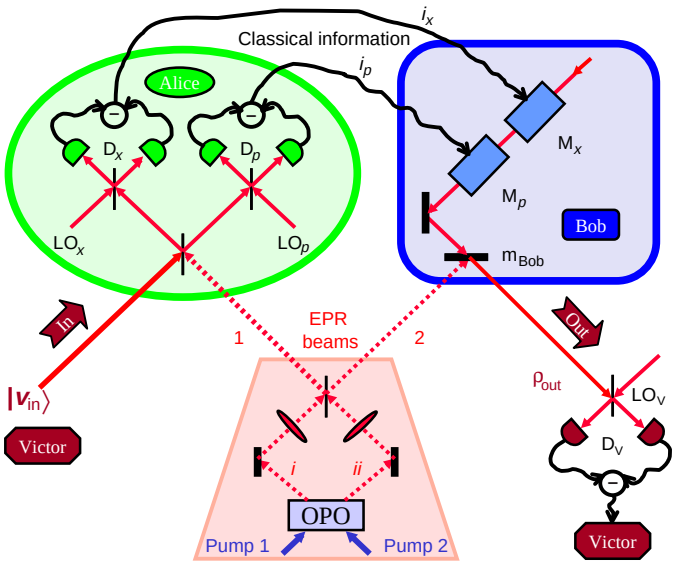

Fig. 1. Schematic of the experimental apparatus for teleportation of an unknown quantum state $|v_{in}\rangle$ from Alice's sending station to Bob's receiving terminal by way of the classical information (i_x, i_p) sent from Alice to Bob and the shared entanglement of the EPR beams (1, 2).

limit of perfect teleportation (for which $\sigma^{-}_{i,ii} \rightarrow 0$, $\sigma^{+}_{i,ii} \rightarrow \infty$, and hence the variance σ_1 of the EPR beam 1 diverges).

The various spectral densities displayed in Fig. 2 are directly related to the means and variances of the quadrature-phase amplitudes of the incident fields (*17, 19*). Because we are dealing with broad-bandwidth fields, the single-mode treatment of (*10*) must be generalized to the case of multimode fields of finite bandwidth (*29*). In this situation, the relevant quantities are the spectral components ($x(\Omega)$, $p(\Omega)$) of the QAs, where a general QA at phase δ is defined by

$$z(\Omega,\delta) \equiv \int_{\Omega-\Delta\Omega}^{\Omega+\Delta\Omega} d\Omega' [\hat{a}(\Omega') \exp(-i\delta) + \hat{a}^{\dagger}(-\Omega') \exp(+i\delta)] \quad (3)$$

with $\hat{a}(\hat{a}^{\dagger})$ as the annihilation (creation) operator for the field at offset Ω from the optical carrier, with $(x(\Omega), p(\Omega)) = (z(\Omega, 0), z(\Omega, \pi/2))$, and with the integration extending over a small interval ΔΩ about Ω. We then have

$$\Psi(\Omega)\Delta\Omega \sim \langle z^2(\Omega,\delta)\rangle \quad (4)$$

(*15, 17*). As shown in (*29*), the teleportation protocol of (*10*) remains unchanged in its essential character. However, now the state being teleported describes the field at frequency offset $\pm\Omega$ within a bandwidth ΔΩ about the carrier ω_L (that is, AM and FM modulation sidebands), with FM sidebands applied by Victor to create the input $v_{in}(\Omega)$.

Given Alice's measurement of $(x(\Omega), p(\Omega))$, the next step in the protocol is for her to send the (classical) photocurrents $(i_x(\Omega), i_p(\Omega))$ to Bob, who uses this information to generate a displacement (a coherent modulation at Ω) of the field in beam 2 by way of the modulators (M_x, M_p) and the mirror m_{Bob}. Note that the phases of both Alice's and Bob's fields relative to the EPR beams {1, 2} are fixed by servo-control. Bob's action results in the teleported output field, which is subsequently interrogated by Victor by way of his own (independent) balanced homodyne detector. Shown in Fig. 3 is Victor's measurement of the QAs of the teleported field, as expressed by the spectral density of photocurrent fluctuations $\Psi^{Victor}(\Omega)$ as a function of time, again as the phase ϕ_{in} is linearly swept. Here, the gain is $g = 1$ (that is, 0 dB), so that Victor's signal level rises 3 dB above that in Fig. 2A, in correspondence to a reconstruction of the coherent amplitude $v_{in}(\Omega) \rightarrow v_{out}(\Omega)$ for the output field. This transformation is independent of the phase of the input field relative to Alice's detectors (D_x, D_p) and to the consequent division of this amplitude to Bob's modulators (M_x, M_p), so that the phase of the teleported field tracks that of the input. In the particular case of Fig. 3A, the phase ϕ_{Victor} of Victor's local oscillator is servo-controlled relative to Alice's and Bob's fields, but it can as well be freely scanned. As in Fig. 2, the phase-insensitive noise levels in Fig. 3A correspond to the case of a vacuum-state input $v_{in} = 0$, first with no EPR beams present (that is, classical teleportation with $\sigma^{\pm}_{i,ii} \rightarrow 1$), giving the level $Y_0^{Victor}(\Omega)$, and then to quantum teleportation with the EPR beams {1, 2} distributed to Alice and Bob, giving $\Lambda^{Victor}(\Omega)$. These noise levels are shown in somewhat more detail in Fig. 3B.

For $g = 1$ (0 dB), as here, the level Y_0^{Victor} stands ~4.8 dB above Victor's vacuum-state level Φ_0^{Victor}, in correspondence to the three units of vacuum noise previously discussed. However, in contradistinction to the increases $\Phi^{Alice}_{0,(x,p)} \rightarrow \Lambda^{Alice}_{(x,p)}$ recorded by Alice, Victor observes a decrease in fluctuations $Y_0^{Victor} \rightarrow \Lambda^{Victor}$ brought about by the presence of the EPR beams, indicating the success of the teleportation protocol. More quantitatively, for $g = 1$, Victor observes a decrease of $10[\log \Lambda^{Victor}(\Omega) - \log Y_0^{Victor}(\Omega)] = -1.2 \pm 0.2$ dB. The ratio $\Lambda^{Victor}(\Omega)/\Phi_0^{Victor}(\Omega)$ then leads directly to the variance $\sigma_W = 2.23 \pm 0.03 < \sigma_W^c = 3$ for the teleported field.

Demonstration of quantum teleportation. By carrying out a series of measurements similar to those shown in Figs. 2 and 3, we have explored the dependence of both the variance of the teleported field and the fidelity F on Bob's gain g. Plotted in Fig. 4 as a function of g are the variances $\sigma_W^{x,p}$ obtained by Victor at D_V for

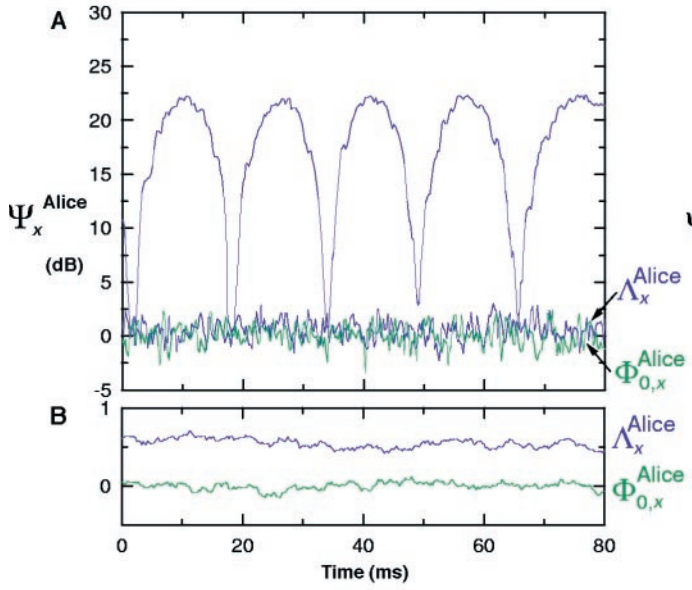

Fig. 2 (left). (**A**) Spectral density of photocurrent fluctuations $\Psi_x^{Alice}(\Omega)$ recorded by Alice's balanced homodyne detector D_x as a function of time with the phase ϕ_{in} of the coherent-state input linearly swept. For the case of a vacuum-state input $v_{in} = 0$ and with no EPR beams present, the vacuum-state level $\Phi_{0,x}^{Alice}(\Omega)$ results, whereas with $v_{in} = 0$ and EPR beam 1 distributed to Alice, excess noise at the level $\Lambda_x^{Alice}(\Omega)$ is recorded. (**B**) Expanded view for $v_{in} = 0$, now with a 10-trace average. Acquisition parameters: radio frequency (rf) $\Omega/2\pi = 2.9$ MHz, rf bandwidth $\Delta\Omega/2\pi = 30$ kHz, video bandwidth = 1 kHz (A) and 30 Hz (B).

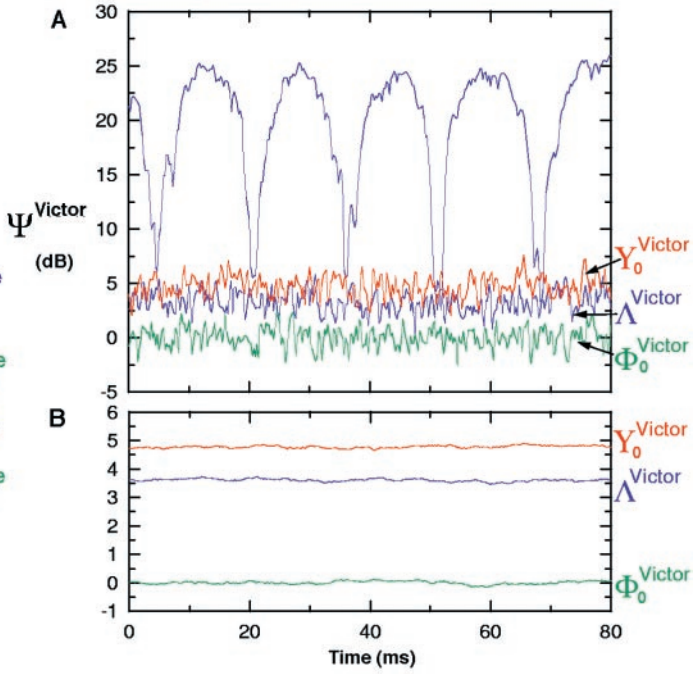

Fig. 3 (right). (**A**) Spectral density of photocurrent fluctuations $\Psi^{Victor}(\Omega)$ recorded by Victor's balanced homodyne detector D_V as afunction of time with the phase ϕ_{in} of the coherent-state input linearly swept and with the gain $g \approx 1$. For the case of a vacuum-state input $v_{in} = 0$ and with no EPR beams present, the excess noise level $Y_0^{Victor}(\Omega)$ results, whereas with $v_{in} = 0$ and EPR beams {1, 2} distributed to Alice and Bob, the level of fluctuations is reduced to $\Lambda^{Victor}(\Omega)$. The vacuum-state level for D_V is given by Φ_0^{Victor}. (**B**) Expanded view for $v_{in} = 0$, now with a 10-trace average. Acquisition parameters are as in Fig. 2.

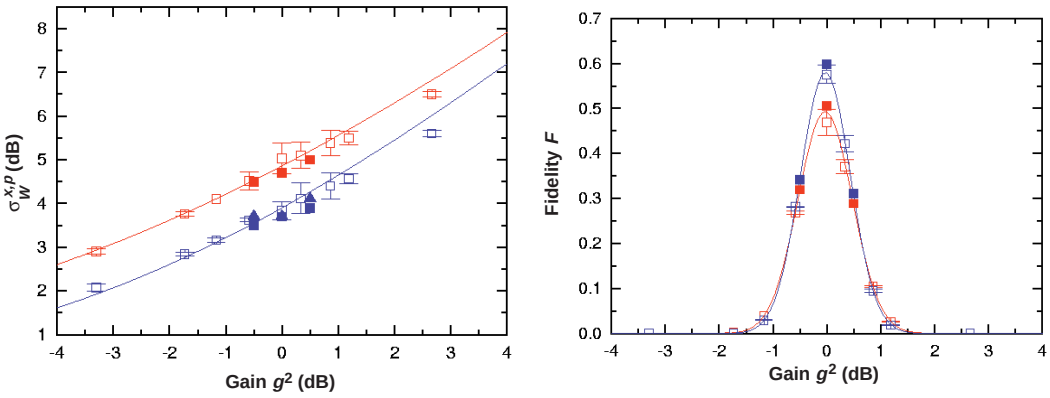

Fig. 4 (left). Variance $\sigma_W^{x,p}$ of the teleported field measured by Victor as a function of the gain g used by Bob for the phase-space displacement of the EPR beam 2. Shown are data obtained both with the quantum-correlated EPR beams present (blue) and with vacuum-state inputs (red) for beams {1, 2}. Open and filled symbols represent results of two different experiments. The theoretical results from Eq. 2 (curves) are also shown for the two cases of quantum and classical teleportation. **Fig. 5 (right).** Fidelity F inferred from measurements of the input amplitude v_{in} and of the quantities v_{out} and $\sigma_Q^{x,p}$ for the teleported output field. Data for the cases of classical (red) and quantum (blue) teleportation are shown, as are the theoretical results from Eq. 1 (curves). See text for explanations of filled and open symbols. $F > 0.5$ demonstrates the nonclassical nature of the protocol.

measurements with the phase ϕ_{Victor} locked to that of Alice's local oscillator at detector D_x (squares) and D_p (triangles), with the open and filled symbols from two different experiments. Comparison of the data in Fig. 4 with the theoretical result from Eq. 2 and the independently measured quantities $\xi_{1,2} = 0.90 \pm 0.04$, $\eta^2 = 0.97 \pm 0.02$, and $\{\sigma^- = 0.5 \pm 0.1, \sigma^+ = 1.8 \pm 0.2\}$ yields reasonable agreement. In particular, the EPR beams bring a reduction of $\sigma_W^{x,p}$ below the limit σ_W^c for classical teleportation with vacuum-state inputs over a reasonably wide range in g. Results similar to these are obtained for σ_W with ϕ_{Victor} swept independent of (D_x, D_p). Note that in a given experiment, we observe a systematic increase in $\sigma_W^p/\sigma_W^x \approx 1.05$, which is presumably associated with asymmetries and non-ideal couplings of the squeezed beams $\{i, ii\}$ that are summed to produce the EPR beams {1, 2} (*17*).

Data as in Fig. 4, together with a record of the mean coherent amplitude $\beta_{out}(\Omega) = gv_{in}(\Omega)$ measured by Victor for the teleported field, allow us to infer the fidelity by way of a simple generalization of Eq. 1, namely

$$F = \frac{2}{\sqrt{\sigma_Q^x \sigma_Q^p}} \exp\left(-2|v_{out} - v_{in}|^2 \Big/ \sqrt{\sigma_Q^x \sigma_Q^p}\right) \quad (5)$$

Here, $\sigma_Q^{x,p} \equiv (1 + \sigma_W^{x,p})$ are the variances for the Q function obtained by Victor from measurements of the spectral densities of photocurrent fluctuations (that is, without correction for his detection efficiencies). Again under the assumption of Gaussian statistics for the teleported field, we thus deduce F, with the results shown in Fig. 5. The filled points around $g = 1$ (0 dB) are from independent measurements of $\sigma_W^{x,p}$, whereas for the open symbols, we approximate $\sigma_W^p \approx 1.05\sigma_W^x$, as above. The theoretical curve is from Eq. 1 with the aforementioned values $\xi_{1,2}$, η, and $\sigma^{\pm}$. Although the agreement between theory and experiment is evidently quite reasonable, the essential observations are that (i) the fidelity for classical teleportation with $\sigma_{i,ii}^{\pm} = 1$ is found to be $F_c^{exp} = 0.48 \pm 0.03 < F_c$, and (ii) the fidelity for quantum teleportation is $F_q^{exp} = 0.58 \pm 0.02 > F_c$. Recall that $F_c = 0.5$ is the classical bound attainable by Alice and Bob in the absence of shared entanglement (*14*), so that $F_q^{exp} > F_c$ demonstrates the nonclassical nature of the experiment.

By exploiting squeezed-state entanglement, we have the first realization of quantum teleportation as originally proposed in (*1*): An unknown quantum state input to Alice's station is transported to a field recreated at Bob's remote station. The quantum nature of the protocol is demonstrated with reference to both the variance σ_W of the teleported field and its fidelity F relative to the original input state, where we emphasize that σ_W and F relate to a physical field emerging from Bob's station. Because we have made no correction for the finite efficiency of Victor's detection process, the fidelity of the actual teleported field is higher than that quoted. Even without such correction, the overall efficiency of our scheme, together with the shared entanglement of the EPR beams, ensure full quantum teleportation: A quantum state presented at the input is teleported with nonclassical fidelity on each and every trial (of duration given by the inverse bandwidth $1/\Delta\Omega$). This high-efficiency experimental implementation of a quantum algorithm for continuous variables suggests that other protocols, including quantum error correction (*12*) and superdense coding (*13*) of optical fields, are not far from realization.

References and Notes

1. C. H. Bennett *et al.*, *Phys. Rev. Lett.* **70**, 1895 (1993).
2. J. S. Bell, *Speakable and Unspeakable in Quantum Mechanics* (Cambridge Univ. Press, New York, 1988), p. 196.
3. L. Davidovich *et al.*, *Phys. Rev. A* **50**, R895 (1994).
4. J. I. Cirac and A. S. Parkins, *ibid.*, p. R4441.
5. T. Sleator and H. Weinfurter, *Ann. N.Y. Acad. Sci.* **755**, 715 (1995).
6. S. L. Braunstein and A. Mann, *Phys. Rev. A* **51**, R1727 (1995); *ibid.* **53**, 630 (1996).
7. D. Boschi *et al.*, *Phys. Rev. Lett.* **80**, 1121 (1998).
8. D. Bouwmeester *et al.*, *Nature* **390**, 575 (1997).
9. L. Vaidman, *Phys. Rev. A* **49**, 1473 (1994).
10. S. L. Braunstein and H. J. Kimble, *Phys. Rev. Lett.* **80**, 869 (1998).
11. B. Yurke, S. L. McCall, J. R. Klauder, *Phys. Rev. A* **33**, 4033 (1986).
12. S. L. Braunstein, *Nature* **394**, 47 (1998).
13. ——— and H. J. Kimble, in preparation.
14. S. L. Braunstein, C. A. Fuchs, H. J. Kimble, in preparation.
15. M. D. Reid and P. D. Drummond, *Phys. Rev. Lett.* **60**, 2731 (1988); M. D. Reid, *Phys. Rev. A* **40**, 913 (1989).
16. A. Einstein, B. Podolsky, N. Rosen, *Phys. Rev.* **47**, 777 (1935).
17. Z. Y. Ou, S. F. Pereira, H. J. Kimble, K. C. Peng, *Phys. Rev. Lett.* **68**, 3663(1992); Z. Y. Ou, S. F. Pereira, H. J. Kimble, *Appl. Phys. B* **55**, 265 (1992).
18. S. L. Braunstein and H. J. Kimble, *Nature* **394**, 840 (1998).
19. H. J. Kimble, in *Fundamental Systems in Quantum Optics, Les Houches, Session LIII, 1990*, J. Dalibard, J. M. Raimond, J. Zinn-Justin, Eds. (Elsevier, Amsterdam, 1992), pp. 549–674.
20. L. A. Wu *et al.*, *Phys. Rev. Lett.* **57**, 2520 (1986).
21. E. S. Polzik, J. Carri, H. J. Kimble, *ibid.* **68**, 3020 (1992); *Appl. Phys. B* **55**, 279 (1992).
22. E. S. Polzik and H. J. Kimble, *Opt. Lett.* **16**, 1400 (1991).
23. E. Arthurs and J. L. Kelly Jr., *Bell. Syst. Tech. J.* (April), 725 (1965).
24. H. P. Yuen and J. H. Shapiro, *IEEE Trans. Inf. Theory* **IT-26**, 78 (1980).
25. S. L. Braunstein, *Phys. Rev. A* **42**, 474 (1990).
26. Related work involves feedforward manipulation of twin-beam states [P. R. Tapster, J. G. Rarity, J. S. Satchell, *Phys. Rev. A* **37**, 2963 (1988); J. C. Mertz *et al.*, *Phys. Rev. Lett.* **64**, 2897 (1990)].
27. C. A. Fuchs and A. Peres, *Phys. Rev. A* **53**, 2038 (1996).
28. H. Barnum, thesis, University of New Mexico (1998).
29. P. van Loock, S. L. Braunstein, H. J. Kimble, in preparation.

30. The experiment was carried out in the Quantum Optics Group at the California Institute of Technology. Supported by the Quantum Information and Computation Institute funded by the Defense Advanced Research Projects Agency via the Army Research Office, by the Office of Naval Research, and by NSF. A.F. is a visiting scientist from the Nikon Research Laboratories. S.L.B. was funded in part by Engineering and Physical Sciences Research Council (UK) grant GR/L91344. C.A.F. also acknowledges support from a Lee A. DuBridge Fellowship. J.L.S. and E.S.P. acknowledge support from the Danish Research Council. We gratefully acknowledge the contributions of N. Ph. Georgiades and discussions with C. M. Caves, N. Cohen, S. J. van Enk, and H. Mabuchi.

20 July 1998; accepted 2 September 1998